



Flow boiling heat transfer in two-phase micro-channel heat sinks—II. Annular two-phase flow model

Weilin Qu, Issam Mudawar *

Boiling and Two-phase Flow Laboratory, School of Mechanical Engineering, Purdue University, 1288 Mechanical Engineering Building, West Lafayette, IN 47907-1288, USA

Received 27 September 2002; received in revised form 13 January 2003

Abstract

This paper is Part II of a two-part study devoted to measurement and prediction of the saturated flow boiling heat transfer coefficient in water-cooled micro-channel heat sinks. Part I discussed the experimental findings from the study, and identified unique aspects of flow boiling in micro-channels such as abrupt transition to the annular flow regime near the point of zero thermodynamic equilibrium quality, and the decrease in heat transfer coefficient with increasing quality. The operating conditions of water-cooled micro-channels fell outside the recommended range for most prior empirical correlations. In this paper, an annular flow model is developed to predict the saturated flow boiling heat transfer coefficient. Features unique to two-phase micro-channel flow, such as laminar liquid and vapor flow, smooth interface, and strong droplet entrainment and deposition effects, are identified and incorporated into the model. The model correctly captures the unique overall trend of decreasing heat transfer coefficient with increasing vapor quality in the low vapor quality region of micro-channels. Good agreement is achieved between the model predictions and heat transfer coefficient data over broad ranges of flow rate and heat flux.

© 2003 Elsevier Science Ltd. All rights reserved.

1. Introduction

Accurate prediction of the flow boiling heat transfer coefficient in micro-channel heat sinks has recently emerged as a critical design need for a number of cutting-edge technologies. Many of these technologies share a common requirement of intense heat removal from very small areas, often with very stringent constraints on the volume available for packaging cooling hardware, including coolant inventory. Thermal design engineers commonly resort to using any number of empirical heat transfer correlations that have been developed over nearly five decades for mostly nuclear, conventional power generation and petroleum industries.

Empirical correlations are a convenient means for determining the flow boiling heat transfer coefficient

using an explicit function of measurable parameters. Like most two-phase flow correlations, heat transfer correlations are developed from experimental databases that are either measured by the author(s) of a correlation, compiled from the literature, or both. In either case, a correlation is valid only for the specific flow configuration and operating conditions the database is based upon. Caution must therefore be exercised when applying a correlation to conditions beyond those for which it was originally developed, and it is often necessary to carry out a careful assessment of the correlation beforehand to explore its suitability to new flow configurations or operating conditions. Failure to conduct such an assessment is a primary cause of uncertainty in designing new systems, which can lead to catastrophic design failure.

Those concerns are particularly important to the topic of this study, since technical know-how of two-phase micro-channel heat sinks is still in its infancy. High-flux heat sinks possess several unique features not commonly found in conventional systems. These

* Corresponding author. Tel.: +1-765-494-5705; fax: +1-765-494-0539.

E-mail address: mudawar@ecn.purdue.edu (I. Mudawar).

tube geometry often used in those studies, and reliance on mostly refrigerants to correlate experimental data. As indicated in Part I, refrigerants feature small bubble departure diameter, allowing nucleate boiling to prevail over an appreciable portion of the saturated flow region of a mini/micro-channel. Greater surface tension and contact angle result in much larger vapor bubbles in water compared to most common refrigerants, which, for a micro-channel, lead to abrupt transition to the annular flow regime close the point of zero thermodynamic equilibrium quality. Thus, new predictive tools are now needed to tackle the design and performance assessment of water-cooled micro-channel heat sinks.

Where possible, theoretical flow-pattern-based models are the preferred alternative to empirical heat transfer correlations. For flow boiling in channels, the liquid and vapor phases can assume one of several flow patterns such as bubbly, slug, and annular. The prevailing pattern is of paramount importance to the mechanism of heat transfer to the coolant and, therefore, has a strong bearing on the magnitude of the heat transfer coefficient. Numerous studies have been conducted in pursuit of theoretical two-phase flow models that incorporate the characteristics of the dominant flow pattern. Such flow-pattern-based models provide a more realistic description of the various transport processes in the two-phase region, from which important hydrodynamic and thermal parameters such as pressure gradient and the heat transfer coefficient may be derived. Compared to empirical correlations, a flow-pattern-based model is more physically sound and therefore may have a broader application range. It is the specific purpose of this paper to explore the application of this alternative approach to predicting the saturated flow boiling heat transfer coefficient in water-cooled micro-channel heat sinks.

Flow visualization studies have been performed on water flow boiling in the present micro-channel heat sink, and results were reported in a separate paper by the authors [2]. These studies indicate the dominant flow pattern under high-heat-flux conditions is annular flow with a large amount of liquid droplets entrained in the vapor core. This conclusion is supported by several previous visualization studies as well [3,4]. The annular flow pattern is therefore adopted in this paper as a basis for constructing the two-phase flow model.

Annular two-phase flow models have been successfully employed for prediction of the heat transfer coefficient, pressure drop, and critical heat flux in numerous applications involving macro-scale boiling and two-phase flow. The general characteristics of annular two-phase flow have been discussed by Hewitt and Hall-Taylor [5] and Hewitt [6]. While annular flow models have not been applied to two-phase micro-channel heat sinks, a few investigators have successfully implemented such models in somewhat related applications such as

narrow channels with serrated fins [7] and small channels with offset strip fins [8,9].

This paper is Part II of a two-part study devoted to the understanding and modeling the saturated flow boiling heat transfer coefficient in a water-cooled two-phase micro-channel heat sink. Part I of this study [1] discussed the experimental methods used and key trends of the heat transfer coefficient with mass velocity and thermodynamic equilibrium quality. Also included in Part I was the aforementioned assessment of previous empirical correlations. This paper focuses on constructing an annular two-phase flow model specifically tailored to micro-channels, which can improve the accuracy of predicting both the overall parametric trends and magnitude of the saturated boiling heat transfer coefficient. The unique features of micro-channel flow boiling discussed in Part I are carefully identified and incorporated into the model. General hydrodynamic characteristics of the micro-channel annular flow are first discussed, followed by application of conservation equations to the regions occupied by each phase. Solving these equations is shown to capture the detailed fluid flow and thermal characteristics of the micro-channel, from which the heat transfer coefficient is evaluated. This paper is concluded with an assessment of the model's predictive capability using the experimental results from Part I.

2. Annular flow model

Fig. 1(a) illustrates the general hydrodynamic characteristics of annular flow in a two-phase micro-channel heat sink. The vapor phase flows along the center of the channel as a continuous vapor core. The liquid phase is

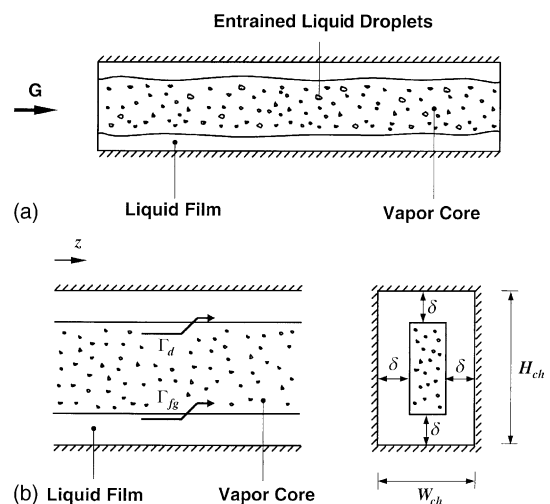


Fig. 1. (a) Schematic of annular flow pattern in micro-channel heat sink, and (b) idealized annular flow region.

comprised of two portions: a thin annular film along the channel wall, and droplets that are entrained in the vapor core. Mass is continuously exchanged between the liquid film and vapor core along the direction of fluid flow.

Several simplifying assumptions are adopted in the model development, which can be summarized as follows:

- (1) The two-phase flow is steady.
- (2) The vapor quality in the annular flow region is equal to the thermodynamic equilibrium quality.
- (3) Pressure is uniform across the micro-channel cross-sectional area.
- (4) The vapor core is comprised of a homogeneous mixture of vapor and entrained droplets. The temperature of the two-phase mixture within the vapor core is equal to the saturation temperature based on local pressure.
- (5) Evaporation occurs only at the interface between the liquid film and vapor core, and the interface temperature is equal to the saturation temperature based on local pressure. Evaporation of liquid droplets in the vapor core is neglected because of both the relative remoteness of the droplets from the heated wall and very short residence time of droplets in a micro-channel heat sink.
- (6) The thickness of the annular liquid film is uniform along the channel circumference, and small compared to the hydraulic diameter.
- (7) Fluid flow in both the liquid film and vapor core is laminar. This assumption, which will be verified later in this paper, is based on the characteristics of low coolant flow rate and small channel size inherent to micro-channel heat sinks.
- (8) The interface between the liquid film and vapor core is fairly smooth due to the relatively strong influence of surface tension in small channels. It is also postulated any interfacial instabilities, including both small wavelength ripples and large wavelength disturbance waves at the liquid film interface are suppressed.
- (9) Entrainment of liquid droplets into the vapor core takes place entirely at the onset of annular flow regime development. Droplet entrainment due to break-up of disturbance waves at the liquid film interface is insignificant with a smooth interface.
- (10) There is continuous deposition of droplets from the vapor core to the liquid film interface along the stream-wise direction. Droplet deposition rate per unit area is assumed uniform along the channel perimeter.

A single micro-channel is examined in the model development. Symmetry allows results for this representative channel to be easily extended to the entire

micro-channel heat sink. Adoption of the aforementioned approximations leads to the simplified geometrical representation of the annular flow pattern illustrated in Fig. 1(b). Γ_{fg} and Γ_d in this figure are the rates of mass transfer by evaporation and deposition, respectively, per unit channel length.

The liquid film mass flow rate, \dot{m}_{Ff} , liquid film thickness, δ , pressure gradient, $-(dP/dz)$, and interfacial shear stress, τ_i , constitute the four primary parameters for the annular two-phase flow model. Other hydrodynamic and thermal parameters, including the heat transfer coefficient, can be evaluated from those primary parameters. Equations relating the primary parameters are established by application of fundamental conservation equations to both the liquid film and vapor core.

2.1. Model construction

2.1.1. Mass conservation

The total mass flow rate, \dot{m} , in the micro-channel is the sum of flow rates of the liquid film, \dot{m}_{Ff} , liquid droplets, \dot{m}_{Ef} , and vapor core, \dot{m}_g

$$\dot{m} = \dot{m}_{Ff} + \dot{m}_{Ef} + \dot{m}_g. \quad (1)$$

The ratio of each portion to the total mass flow rate is defined as liquid film quality, f , liquid droplet quality, e , and vapor quality, x , respectively

$$f = \frac{\dot{m}_{Ff}}{\dot{m}}, \quad (2)$$

$$e = \frac{\dot{m}_{Ef}}{\dot{m}}, \quad (3)$$

and

$$x = \frac{\dot{m}_g}{\dot{m}}. \quad (4)$$

From Eq. (1),

$$f + e + x = 1. \quad (5)$$

From assumption (2), the vapor quality can be evaluated from

$$x = x_e, \quad (6)$$

$$\text{where } x_e = \frac{h - h_f}{h_{fg}}. \quad (7)$$

Two other parameters important in the model development are defined as

$$x_c = \frac{\dot{m}_g}{\dot{m}_{Ef} + \dot{m}_g}, \quad (8)$$

and

$$F_c = \frac{\dot{m}_{Ef}}{\dot{m}_{Ff} + \dot{m}_{Ef}}, \quad (9)$$

where x_c is the effective vapor quality in the vapor core, and F_c the fraction of liquid flow rate entrained as droplets in the vapor core.

Taking into account the transfer of mass between the liquid film and vapor core, the following mass conservation equations can be established,

$$\frac{d\dot{m}_{Ff}}{dz} = -\Gamma_{fg} + \Gamma_d, \tag{10}$$

$$\frac{d\dot{m}_{Ef}}{dz} = -\Gamma_d, \tag{11}$$

and

$$\frac{d\dot{m}_g}{dz} = \Gamma_{fg}. \tag{12}$$

The rate of mass transfer due to evaporation can be related to the effective heat flux by the relation

$$\Gamma_{fg} = \frac{q''_{eff} W}{N h_{fg}}. \tag{13}$$

The rate of mass transfer due to deposition can be expressed as

$$\Gamma_d = DP_c, \tag{14}$$

where P_c is the perimeter of the vapor core,

$$P_c = 2[(W_{ch} - 2\delta) + (H_{ch} - 2\delta)], \tag{15}$$

and D the deposition rate based on circumferential area of the vapor core. In the literature, droplet deposition from the vapor core to the annular liquid film is considered a mass transfer process driven by concentration difference [10–12]. The following equation is therefore employed to evaluate the deposition rate D ,

$$D = kC, \tag{16}$$

where C is the liquid droplet concentration in the vapor core,

$$C = \frac{\dot{m}_{Ef}}{\dot{m}_g v_g + \dot{m}_{Ef} v_f}, \tag{17}$$

and k the deposition mass transfer coefficient. Due to the complexity of this process, researchers have relied on empirical methods to determine the deposition mass transfer coefficient [10–12]. Results are often unsatisfactory, evidenced by large discrepancies between model predictions of the heat transfer coefficient and experimental data. Complicating the task of estimating k is the reliance of most available correlations on adiabatic air–water two-phase flow experiments in large tubes, which may not be suitable for the present micro-channel flow boiling configuration. To overcome this difficulty, a new correlation is proposed in the present study to facilitate

close agreement between the present model predictions and experimental results. The new correlation is expressed as

$$\frac{k}{j_g} = 47.8Bo \left(\frac{C}{\rho_g} \right)^{-0.147}, \tag{18}$$

where Bo is the boiling number based on mean heat flux along the heated perimeter,

$$Bo = \frac{q''_{eff} W}{N(W_{ch} + 2H_{ch})Gh_{fg}} \tag{19}$$

and j_g the vapor superficial velocity given by

$$j_g = \frac{\dot{m}_g}{\rho_g A_{ch}}. \tag{20}$$

The functional form of Eq. (18) is based on a correlation originally proposed by Paleev and Filippovich [10] that was modified here by introduction of the boiling number to account for flow boiling effects.

Once Γ_{fg} and Γ_d are specified, Eqs. (10)–(12) may be integrated along the stream-wise direction to obtain local values for \dot{m}_{Ff} , \dot{m}_{Ef} , and \dot{m}_g , given appropriate boundary conditions. The boundary conditions for Eqs. (10)–(12) involve location of the onset of annular flow and the initial mass flow rate of each portion of the micro-channel mass flow rate at that location. In the present study, the criterion for transition to annular flow in horizontal tubes proposed by Taitel and Duckler [13,14] is used to determine the location of the onset of annular flow. This criterion uses a constant value for the Martinelli parameter at the transition point.

$$X_{vv0} = 1.6, \tag{21}$$

where the Martinelli parameter for the combination of laminar liquid and laminar vapor flow is given by

$$X_{vv} = \left(\frac{\mu_f}{\mu_g} \frac{1-x}{x} \frac{v_f}{v_g} \right)^{1/2}. \tag{22}$$

Eqs. (21) and (22) yield a vapor quality x_0 at the onset of annular flow ranging from 0.006 to 0.0064, depending on the fluid properties for a particular test.

Literature review reveals determination of an initial mass flow rate for each portion of the mass flow rate at the onset of annular flow is somewhat arbitrary. A common practice is to assume a value for the fraction of entrained liquid for a given vapor quality. For instance, Whalley et al. [15] set an initial value for the fraction of liquid entrained as droplets in the vapor core, F_{e0} , of 0.99 for a vapor quality of $x_0 = 0.01$. Recently, Barbosa et al. [16] proposed an alternative correlation in which F_{e0} is a linear function of the square of hydraulic diameter. Their correlation, which is based on macro-channels,

was deemed unsuitable for very small hydraulic diameters since it predicts unrealistically small values for F_{e0} .

Initial numerical results using the present model proved the value proposed by Whalley et al. [15] is an acceptable approximation, but had to be modified to account for the effects of the mass velocity. In addition, surface tension force is believed to play an important role in the initial entrainment process in a micro-channel. Both effects were incorporated in the following expression for initial liquid entrainment quality,

$$e_0 = 0.951 - 0.15\sqrt{We_{f0}}, \quad (23)$$

where We_{f0} is the Weber number defined as

$$We_{f0} = \frac{G^2 d_h v_f}{\sigma}. \quad (24)$$

2.1.2. Momentum conservation in liquid film

Momentum conservation is applied to the liquid film using the control volume shown in Fig. 2(a) and (b). The control volume has the shape of a rectangular ring with a length Δz in the stream-wise direction. The inner

boundary of the control volume extends to the interface between the liquid film and vapor core, and the outer boundary is located within the liquid film a distance y from the channel wall.

Fig. 2(a) illustrates the momentum exchange along the liquid film interface, neglecting any minor momentum changes due to acceleration of the liquid film. The net momentum in the z direction is the difference between evaporation and deposition effects, $\Gamma_{fg} u_i \Delta z - \Gamma_{d} u_c \Delta z$, where u_i is the interfacial velocity, and u_c the mean velocity of the vapor core.

To simplify the model development, the interfacial velocity u_i is set equal to twice the mean liquid film velocity u_{Ff} ,

$$u_i = 2u_{Ff}, \quad (25)$$

where u_{Ff} is given by

$$u_{Ff} = \frac{\dot{m}_{Ff}}{\rho_f(A_{ch} - A_c)}, \quad (26)$$

A_{ch} and A_c being the cross-sectional areas of the channel and vapor core, respectively.

$$A_{ch} = W_{ch} H_{ch} \quad (27)$$

and

$$A_c = (W_{ch} - 2\delta)(H_{ch} - 2\delta). \quad (28)$$

The approximation given in Eq. (25), which is justified mainly by the small thickness of the liquid film, will be verified later in this paper.

Based on the homogeneous flow assumption for the vapor core, the mean velocity of the vapor core can be evaluated from

$$u_c = \frac{\dot{m}_{Ef} + \dot{m}_g}{\rho_H A_c}, \quad (29)$$

where ρ_H is the homogeneous density of the vapor core,

$$\rho_H = \frac{1}{x_c v_g + (1 - x_c) v_f}, \quad (30)$$

accounting for the entrained droplets.

Forces acting on the same control volume in the stream-wise direction are illustrated in Fig. 2(b). Assuming a small film thickness, the sum of forces in the z direction can be expressed as

$$P(\delta - y)P_{ch} - \left(P + \frac{dP}{dz} \Delta z\right)(\delta - y)P_{ch} + \tau_i P_{ch} \Delta z + \tau P_{ch} \Delta z.$$

The first and second terms in this equation represent the pressure forces, while the third and fourth terms are the shear force in the liquid film and interfacial shear force, respectively.

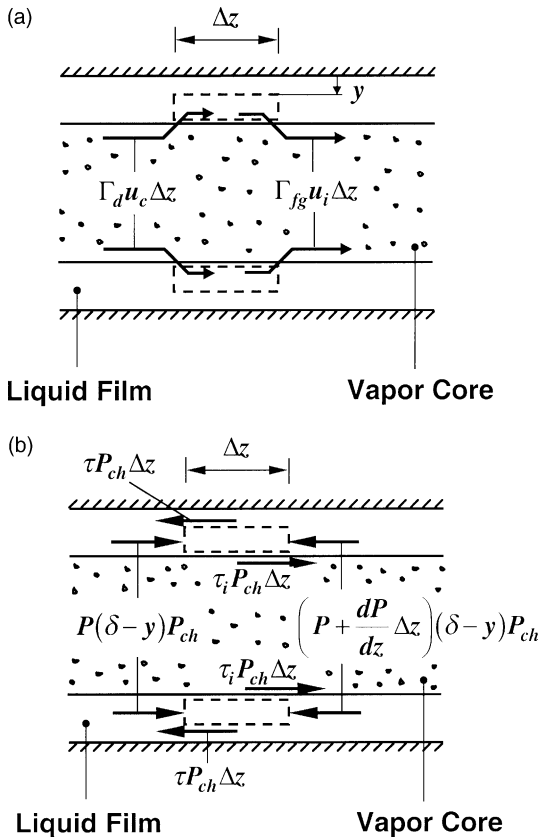


Fig. 2. (a) Momentum interactions and (b) forces acting on liquid film control volume.

Momentum conservation requires the sum of all forces acting on the control volume in the z direction equal the net momentum.

$$\tau = (\delta - y) \left(-\frac{dp}{dz} \right) + \tau_i - \frac{1}{P_{ch}} (\Gamma_{fg} u_i - \Gamma_d u_c). \quad (31)$$

Shear stress in the laminar liquid film is related to the local velocity gradient by

$$\tau = \mu_f \frac{du_f}{dy}. \quad (32)$$

Substituting Eq. (32) into (31) gives

$$\frac{du_f}{dz} = \frac{1}{\mu_f} (\delta - y) \left(-\frac{dp}{dz} \right) + \frac{1}{\mu_f} \tau_i - \frac{1}{\mu_f P_{ch}} (\Gamma_{fg} u_i - \Gamma_d u_c). \quad (33)$$

The local velocity in the liquid film can be obtained by integrating Eq. (33), incorporating the non-slip condition of $u_f = 0$ at $y = 0$

$$u_f = \frac{1}{\mu_f} \left(\delta y - \frac{y^2}{2} \right) \left(-\frac{dp}{dz} \right) + \frac{y}{\mu_f} \tau_i - \frac{y}{\mu_f P_{ch}} (\Gamma_{fg} u_i - \Gamma_d u_c). \quad (34)$$

The liquid film mass flow rate can be determined by integrating the velocity profile across the film thickness

$$\dot{m}_{Ff} = \rho_f P_{ch} \int_0^\delta u_f dy. \quad (35)$$

Substituting Eq. (34) into Eq. (35) and integrating yield

$$\dot{m}_{Ff} = \frac{P_{ch} \rho_f \delta^3}{3\mu_f} \left(-\frac{dp}{dz} \right) + \frac{P_{ch} \rho_f \delta^2}{2\mu_f} \tau_i - \frac{\rho_f \delta^2}{2\mu_f} (\Gamma_{fg} u_i - \Gamma_d u_c). \quad (36)$$

Eq. (36) can be re-arranged to obtain the following relation for pressure gradient for the liquid film,

$$\left(-\frac{dp}{dz} \right) = \frac{3\mu_f}{P_{ch} \rho_f \delta^3} \dot{m}_{Ff} - \frac{3}{2\delta} \tau_i + \frac{3}{2\delta P_{ch}} (\Gamma_{fg} u_i - \Gamma_d u_c). \quad (37)$$

2.1.3. Momentum conservation in vapor core

Fig. 3(a) and (b) show a control volume of length of Δz encompassing the homogeneous vapor core and extending to the liquid film interface. As illustrated in Fig. 3(a), the net momentum for this control volume can be expressed as

$$\left[\rho_H u_c^2 A_c + \frac{d}{dz} (\rho_H u_c^2 A_c) \Delta z \right] - \rho_H u_c^2 A_c + \Gamma_d u_c \Delta z - \Gamma_{fg} u_i \Delta z.$$

The first two terms represent the momentum change due to core acceleration, while the third and fourth terms account for droplet deposition and interfacial evaporation, respectively.

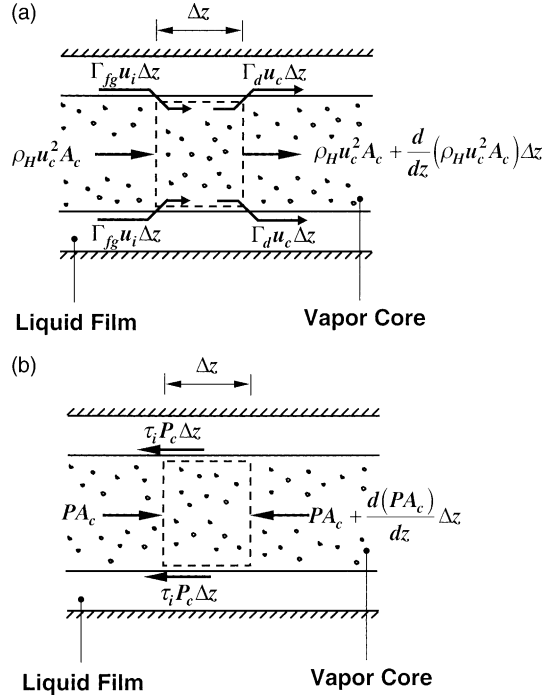


Fig. 3. (a) Momentum interactions and (b) forces acting on vapor core control volume.

Fig. 3(b) shows forces acting on the same control volume in the stream-wise direction produce a net force

$$PA_c - \left[PA_c + \frac{d(PA_c)}{dz} \Delta z \right] - \tau_i P_c \Delta z.$$

The first two terms in this expression account for pressure forces, and the third the interfacial shear force.

Equating the net momentum in the z direction to the net force yields the following equation,

$$\tau_i = \frac{1}{P_c} \left[A_c \left(-\frac{dP}{dz} \right) - P \frac{dA_c}{dz} \right] - \frac{1}{P_c} \frac{d}{dz} (\rho_H u_c^2 A_c) + \frac{1}{P_c} (\Gamma_{fg} u_i - \Gamma_d u_c). \quad (38)$$

2.1.4. Interfacial shear stress

An interfacial friction factor is defined as

$$f_i = \frac{\tau_i}{\frac{1}{2} \rho_H (u_c - u_i)^2}, \quad (39)$$

Following the assumptions of laminar vapor core and smooth liquid film interface, a relation proposed by Shah and London [17] is used to evaluate f_i ,

$$f_i Re_c = 24(1 - 1.3553\beta_c + 1.9467\beta_c^2 - 1.7012\beta_c^3 + 0.9564\beta_c^4 - 0.2537\beta_c^5), \quad (40)$$

where β_c is the aspect ratio of the vapor core,

$$\beta_c = \frac{W_{ch} - 2\delta}{H_{ch} - 2\delta}, \quad (41)$$

Re_c the effective vapor core Reynolds number,

$$Re_c = \frac{\rho_H(u_c - u_i)d_{h,c}}{\mu_g}, \quad (42)$$

and $d_{h,c}$ the hydraulic diameter of the vapor core,

$$d_{h,c} = \frac{4A_c}{P_c}. \quad (43)$$

Mass transfer at the interface due to evaporation may have a significant influence on the interfacial friction. This is incorporated in the model by modifying interfacial shear stress using a treatment by Wallis [18],

$$\tau_i = f_i \left[\frac{1}{2} \rho_H (u_c - u_i)^2 \right] - \frac{\Gamma_{fg}}{2P_c} (u_c - u_i). \quad (44)$$

2.1.5. Solution procedure

The model development so far has resulted in a sufficient number of equations to determine local values for all four primary parameters of the annular flow, \dot{m}_{Ff} , δ , $-(dP/dz)$, and τ_i . Unfortunately, these parameters are interrelated, rendering the equations too complex to be solved analytically. A numerical code is therefore developed to solve these equations using the following procedure:

- (1) Eq. (21) is first used to determine the location of the onset (upstream point) of annular flow. The annular flow region in the micro-channel is then identified as the length from that location to the exit. A grid system containing a sufficiently large number of nodes is adopted for the annular flow region. The initial mass flow rates of the liquid film, liquid droplets, and vapor at the onset of annular flow are evaluated using Eqs. (2)–(5), (21) and (23). The solution is initiated from the node next to the upstream boundary node and proceeds downstream.
- (2) At each node, an initial guess is made for liquid film thickness, δ . All other geometrical parameters in the annular flow region can be evaluated using the tentative δ value.
- (3) Eqs. (13) and (14) are used to evaluate Γ_{fg} and Γ_d . Local mass flow rates for all portions of the flow rate, \dot{m}_{Ff} , \dot{m}_{Ef} , and \dot{m}_g are then evaluated from Eqs. (10)–(12).
- (4) The interfacial shear stress τ_i is evaluated from Eq. (44). All other variables in Eq. (44) are evaluated using geometrical parameters determined from step (2) and the mass flow rates from step (3).

- (5) The pressure gradient $-(dP/dz)$ is evaluated by substituting \dot{m}_{Ff} determined from step (3) and τ_i from step (4) into the right-hand-side of Eq. (37).
- (6) The left-hand-side of Eq. (38) is set equal to τ_i evaluated from step (4), and the right-hand-side using $-(dP/dz)$ evaluated from step (5).
- (7) The solution seeks to balance both sides of Eq. (38). If this criterion is not satisfied, a new value of δ is assumed and steps (2)–(6) repeated. When both sides of Eq. (38) are finally in balance, the values of the primary parameters obtained in the last iteration are adopted for that nodal location.
- (8) The code then repeats the same numerical procedure for the next downstream node in pursuit of a balance for Eq. (38) at this new node. This procedure is then repeated by marching downstream until the last node in the annular flow region is reached.

3. Model predictions and assessment

Base on the assumption of a laminar liquid film, the local heat transfer coefficient in the annular flow region can be evaluated from the simple relation

$$h_{tp} = \frac{k_f}{\delta}. \quad (45)$$

In addition to the laminar flow assumption, Eq. (45) implies heat input to the liquid film from the channel wall is transferred entirely to the vapor core through evaporation at the interface. Comprehensive discussion on the validity of Eq. (45) in evaluating the heat transfer coefficient in laminar annular flow has been provided by Hewitt and Hall-Taylor [5], and Collier and Thome [14].

Fig. 4 compares the model predictions and measured saturated flow boiling heat transfer coefficient, h_{tp} , at z_{tc4} as a function of thermodynamic equilibrium quality, x_c , for $T_{in} = 60$ °C and $G = 255$ kg/m² s, where z_{tc4} is the stream-wise location of the fourth heat sink thermocouple and T_{in} the inlet temperature, respectively. All details of the experimental apparatus and methods used to measure h_{tp} are provided in Part I of this study [1], and will not be presented here for brevity. Unlike all prior empirical correlations (see Figs. 7 and 9 in [1]), Fig. 4 shows the present model correctly captures the overall trend of decreasing h_{tp} with increasing x_c in the saturated boiling region.

The overall predictive capability of the present model is illustrated in Fig. 5, which compares the model predictions with all saturated boiling data from part I. All data are located within a $\pm 40\%$ error band with a mean absolute error (*MAE*) of 13.3%. By comparison, the smallest *MAE* from the eleven empirical correlations examined in Part I is 19.3%, and none of these correlation could capture the correct trend of h_{tp} with x_c .

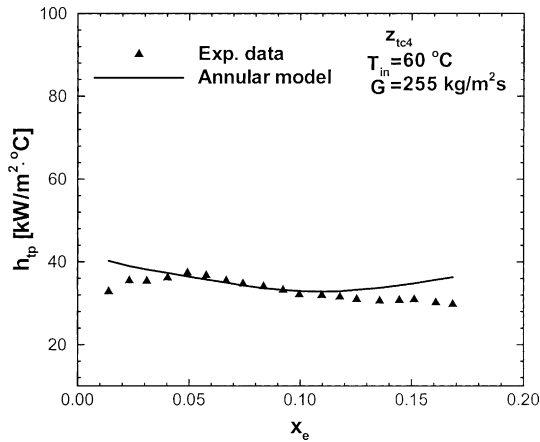


Fig. 4. Comparison of model predictions and saturated flow boiling heat transfer coefficient data at z_{tc4} for $T_{in} = 60\text{ °C}$ and $G = 255\text{ kg/m}^2\text{ s}$.

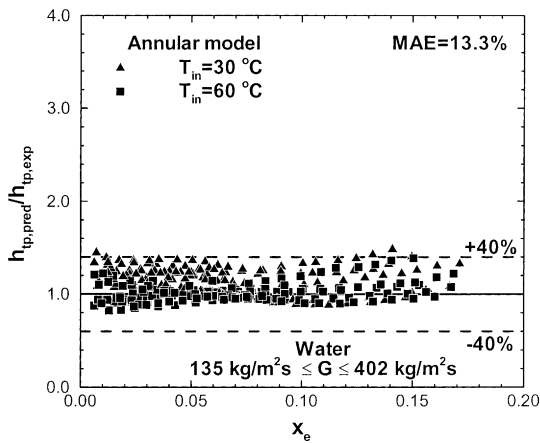


Fig. 5. Comparison of model predictions with all saturated flow boiling heat transfer coefficient data.

Having confirmed the overall accuracy and effectiveness of the model, it is useful to explore some important trends of key parameters of the annular flow as well as justify some of the assumptions outlined at the beginning of the model development.

Fig. 6(a) and (b) show the variation of liquid film quality, f , liquid droplet quality, e , and vapor quality, x , along the stream-wise direction for $T_{in} = 60\text{ °C}$ and $G = 255\text{ kg/m}^2\text{ s}$ at $q''_{eff} = 63$ and 129 W/cm^2 , respectively. The vapor quality, x , increases monotonically due to evaporation resulting from uniform heat input along the flow direction. On the other hand, liquid droplet quality e decreases due to the deposition process and lack of droplet entrainment. At the higher heat flux, e decreases to a very small value in the downstream por-

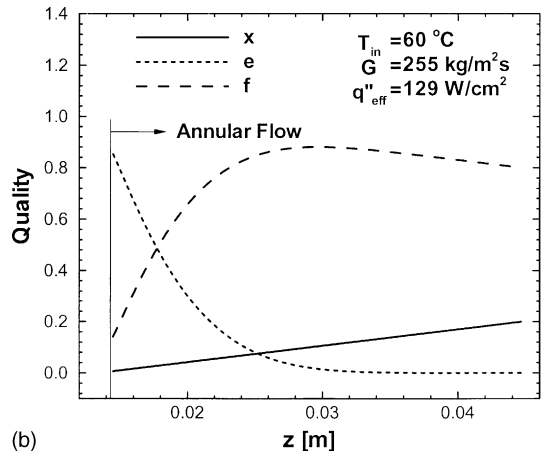
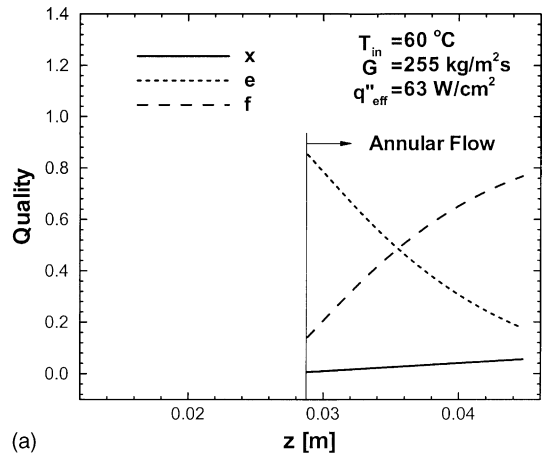


Fig. 6. Variation of liquid film quality, liquid droplet quality, and vapor quality along stream-wise direction for (a) $q''_{eff} = 63\text{ W/cm}^2$ and (b) $q''_{eff} = 129\text{ W/cm}^2$.

tion of the annular flow region. This implies most liquid droplets that were entrained at the onset of annular flow have already been deposited to the liquid film, and the vapor core is comprised of virtually pure vapor downstream. In addition, the liquid film quality, f , increases monotonically in the stream-wise direction at the lower heat flux, indicating deposition is dominant throughout the annular flow region. At the high heat flux, however, f increases at first, and then begins to decrease. This shows deposition is dominant upstream only, and evaporation becomes dominant downstream after most entrained droplets had been deposited to the liquid film.

In the model development, Eq. (25) assumed an interfacial velocity, u_i , twice that of the mean liquid film velocity, u_{Ff} . As indicated previously, this is only an approximation intended to simplify implementation of the numerical solution since the exact value of u_i can be evaluated from Eq. (34).

$$u_i = \left[\frac{1}{\mu_f} \left(\frac{\delta^2}{2} \right) \left(-\frac{dP}{dz} \right) + \frac{\delta}{\mu_f} \tau_i + \frac{\delta}{\mu_f P_{ch}} \Gamma_d u_c \right] / \left(1 + \frac{\delta \Gamma_{fg}}{\mu_f P_{ch}} \right). \quad (46)$$

Fig. 7(a) and (b) show the variation of u_i along the stream-wise direction for $T_{in} = 60\text{ }^\circ\text{C}$, $G = 255\text{ kg/m}^2\text{s}$ at $q''_{eff} = 63$ and 129 W/cm^2 , respectively. Close agreement between the two methods for both heat flux conditions are proof of the validity of the approximation given by Eq. (25).

The distributions of mean liquid film velocity, u_{FF} , and mean vapor core velocity, u_c , along the stream-wise direction are shown in Fig. 8(a) and (b) for $q''_{eff} = 63$ and 129 W/cm^2 , respectively. u_{FF} increases monotonically at the lower heat flux due to entrainment effects. At the high heat flux, however, u_{FF} increases at first, where Fig. 6(a) earlier showed appreciable droplet entrainment, then tapers off to a fairly constant value downstream,

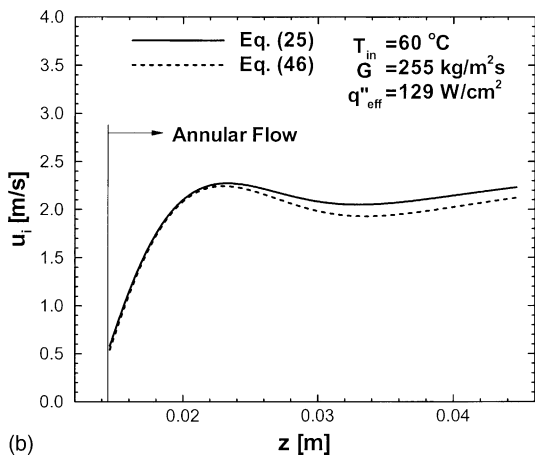
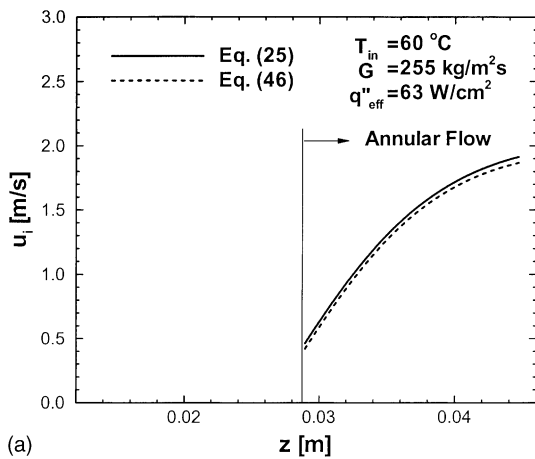


Fig. 7. Variation of interfacial velocity along stream-wise direction for (a) $q''_{eff} = 63\text{ W/cm}^2$ and (b) $q''_{eff} = 129\text{ W/cm}^2$.

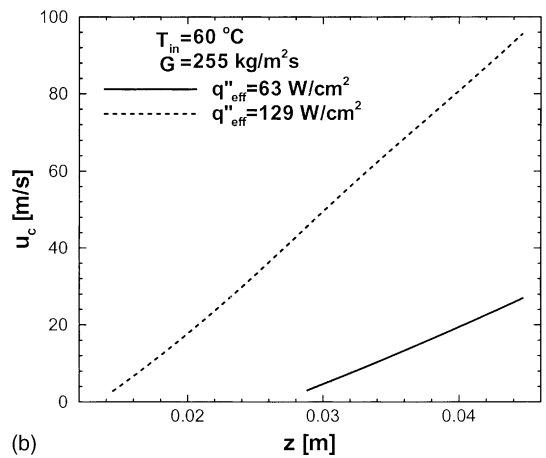
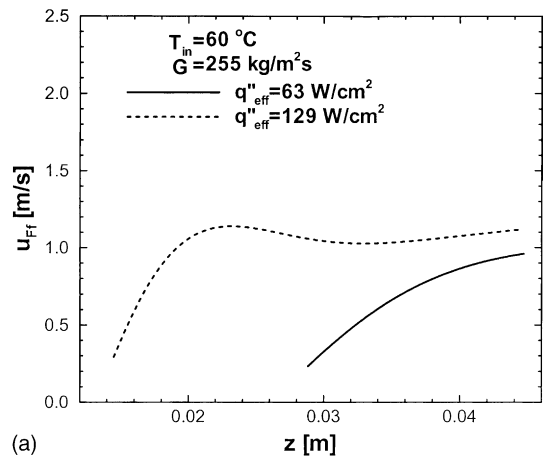


Fig. 8. Variation of (a) mean liquid film velocity and (b) mean vapor core velocity along stream-wise direction.

where entrainment is negligible. On the other hand, u_c increases monotonically in the flow direction for both heat-flux values due to vapor acceleration that accompanies the interfacial evaporation.

Fig. 9 shows the variation of slip ratio

$$S = \frac{u_c}{u_{FF}} \quad (47)$$

for the same conditions as Fig. 8(a) and (b). Both flux cases show a monotonic increase in the z direction, but the combination of higher heat flux and small channel size is shown producing relatively large S values, especially at 129 W/cm^2 .

The distributions of liquid film Reynolds number, Re_{FF} , and vapor core Reynolds number, Re_{cg} , based on vapor phase alone are shown in Fig. 10(a) and (b), respectively, where

$$Re_{FF} = \frac{4\rho_f u_{FF} \delta}{\mu_f} \quad (48)$$

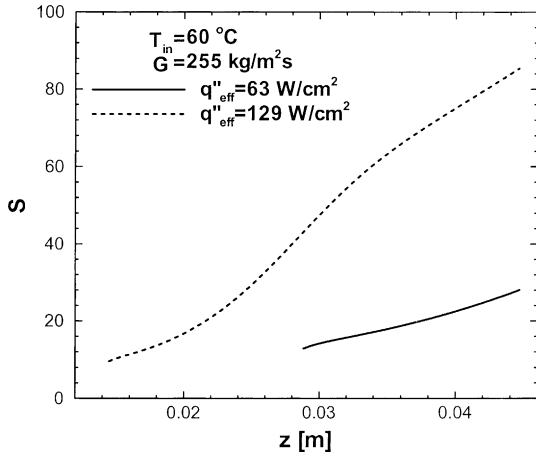


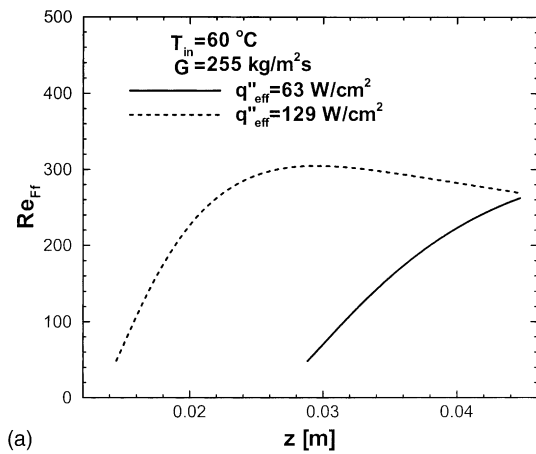
Fig. 9. Variation of slip ratio along stream-wise direction.

and

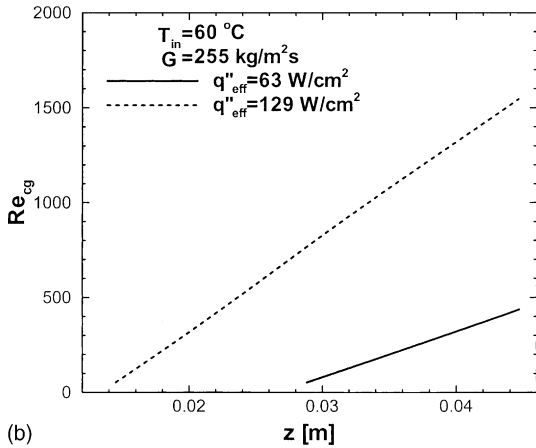
$$Re_{cg} = \frac{\rho_g u_c d_{h,c}}{\mu_g} \quad (49)$$

The relative low values of both Re_{Fr} and Re_{cg} throughout the annular flow region validate the laminar flow assumptions of the present model.

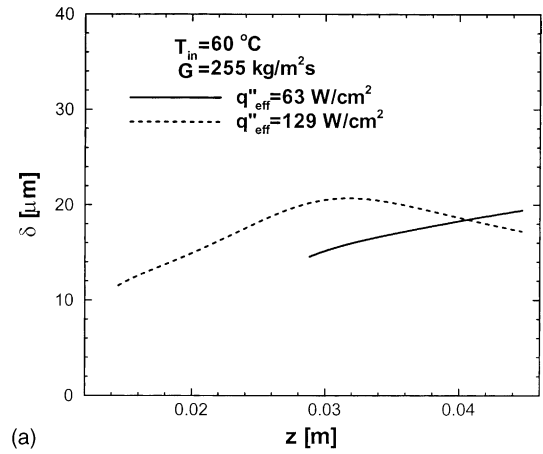
Finally, Fig. 11(a) and (b) show the variations of film thickness, δ , and heat transfer coefficient, h_{tp} , respectively. At the lower heat flux, δ increases monotonically due to the aforementioned dominance of droplet deposition effects. At the high heat flux, δ increases at first due to strong droplet deposition effects, and then begins to decrease slightly because of the large shear force produced by the high velocity vapor core in the evaporation-dominant region. An opposite trend is shown in Fig. 11(b) for h_{tp} , which is simply proportional to $1/\delta$. The effect of entrainment in particular explains the general trend of decreasing h_{tp} with increasing x_e



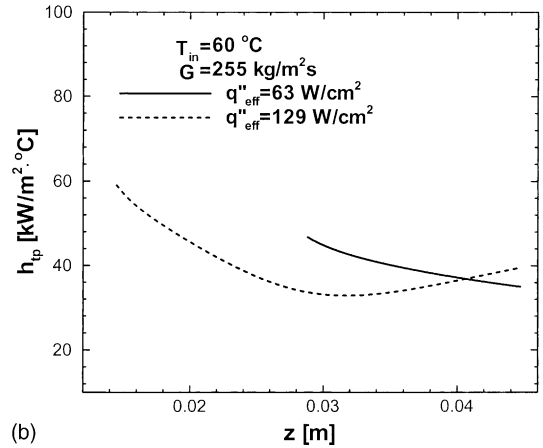
(a)



(b)



(a)



(b)

Fig. 10. Variation of (a) liquid film Reynolds number and (b) vapor core Reynolds number along stream-wise direction.

Fig. 11. Variation of (a) liquid film thickness and (b) saturated two-phase heat transfer coefficient along stream-wise direction.

observed in several micro-channel flow boiling studies as discussed in Part I of this study [1].

4. Conclusions

This paper is Part II of a two-part study devoted to flow boiling heat transfer in a water-cooled micro-channel heat sink. An annular two-phase flow model is developed to predict the saturated flow boiling heat transfer coefficient. Key findings from the study are as follows:

- (1) A new model is developed based on the annular flow pattern identified as the dominant two-phase flow pattern in micro-channel heat sinks. Features unique to two-phase micro-channel flow, such as laminar liquid and vapor flow, smooth interface, and strong droplet entrainment and deposition phenomena, are identified and incorporated into the model. Since no entrainment or deposition correlations are available in the literature for micro-channels, new relations are recommended for both effects.
- (2) The new model is capable of providing a detailed and physically sound description of the various transport processes occurring in two-phase micro-channel heat sinks. Unlike empirical correlation, the annular flow model is better able at depicting interfacial interactions between the phases and therefore has both fundamental appeal and broader application range.
- (3) The new model correctly captures the unique overall trend of decreasing heat transfer coefficient with increasing vapor quality in the low vapor quality region of micro-channels.
- (4) Good agreement is achieved between the model predictions and saturated flow boiling heat transfer coefficient data over broad ranges of flow rate and heat flux. A MAE of 13.3% demonstrates the effectiveness of this model as a design tool for water-cooled two-phase micro-channel heat sinks.
- (5) As the model incorporates empirical elements that are specifically tailored to the unique features of water flow boiling in micro-channels, this model is not recommended for macro-channel flow and its application to conditions beyond those tested in the present study should be subject to further validation.

Acknowledgement

The authors are grateful for the support of the Office of Basic Energy Sciences of the US Department of Energy (Award No. DE-FG02-93ER14394 A7).

References

- [1] W. Qu, I. Mudawar, Flow boiling heat transfer in two-phase micro-channel heat sinks—I. Experimental investigation and assessment of correlation methods, *Int. J. Heat Mass Transfer*, (2003), doi:10.1016/S0017-9310(03)00041-3.
- [2] W. Qu, I. Mudawar, Transport phenomena in two-phase micro-channel heat sinks, *J. Electron. Packaging*, in review.
- [3] L. Zhang, J.M. Koo, L. Jiang, S.S. Banerjee, M. Ashegi, K.E. Goodson, J.G. Santiago, T.W. Kenny, Measurement and modeling of two-phase flow in microchannels with nearly-constant heat flux boundary conditions, in: A. Lee et al. (Eds.), *Micro-Electro-Mechanical Systems (MEMS)—2000*, MEMS-vol. 2, ASME, Orlando, FL, 2000, pp. 129–135.
- [4] L. Jiang, M. Wong, Y. Zohar, Forced convection boiling in a microchannel heat sink, *J. Microelectromech. Syst.* 10 (2001) 80–87.
- [5] G.F. Hewitt, N.S. Hall-Taylor, *Annular Two-Phase Flow*, Pergamon Press, New York, 1970.
- [6] G.F. Hewitt, Prediction of pressure drop in annular flow by phenomenological modeling, in: G. Hetsroni (Ed.), *Handbook of Multiphase Systems*, Hemisphere, Washington, 1981, pp. (2)62–(2)75.
- [7] J.M. Robertson, P.C. Lovegrove, Boiling heat transfer with Freon 11 (R11) in brazed aluminum, plate-fin heat exchangers, *J. Heat Transfer* 105 (1983) 605–610.
- [8] V.P. Carey, G.D. Mandrusiak, Annular film-flow boiling of liquid in a partially heated, vertical channel with offset strip fins, *Int. J. Heat Mass Transfer* 29 (1986) 927–939.
- [9] G.D. Mandrusiak, V.P. Carey, X. Xu, A experimental study of convective boiling in a partially heated horizontal channel with offset strip fins, *J. Heat Transfer* 110 (1988) 229–236.
- [10] I.I. Paleev, B.S. Filippovich, Phenomena of liquid transfer in two-phase dispersed annular flow, *Int. J. Heat Mass Transfer* 9 (1966) 1089–1093.
- [11] G.F. Hewitt, A.H. Govan, Phenomenological modeling of non-equilibrium flows with phase change, *Int. J. Heat Mass Transfer* 33 (1990) 229–242.
- [12] R.I. Nigmatulin, B.I. Nigmatulin, YA.D. Khodzhaev, V.E. Kroschilin, Entrainment and deposition rates in a dispersed-film flow, *Int. J. Multiphase Flow* 22 (1996) 19–30.
- [13] Y. Taitel, A.E. Dukler, A model for predicting flow regime transitions in horizontal and near horizontal gas–liquid flow, *AIChE J.* 22 (1976) 47–55.
- [14] J.G. Collier, J.R. Thome, *Convective Boiling and Condensation*, third ed., Oxford University Press, Oxford, 1994.
- [15] P.B. Whalley, P. Hutchinson, G.F. Hewitt, The calculation of critical heat flux in forced convection boiling, in: *Proceedings of the Fifth International Heat Transfer Conference*, Tokyo, Japan, 1974, Paper B6, pp. 290–294.
- [16] J.R. Barbosa Jr., G.F. Hewitt, G. Konig, S.M. Richardson, Liquid entrainment, droplet concentration and pressure gradient at the onset of annular flow in vertical pipe, *Int. J. Multiphase Flow* 28 (2002) 943–961.
- [17] R.K. Shah, A.L. London, *Laminar Flow Forced Convection in Ducts: a Source Book for Compact Heat Exchanger Analytical Data*, Supl. 1, Academic press, New York, 1978.
- [18] G.B. Wallis, *One Dimensional Two-Phase Flow*, McGraw-Hill, New York, 1969.